Energy distributions at the high-spin ferric sites in myoglobin crystals

Francis G. Fiamingo,* Arthur S. Brill,*‡ Don A. Hampton,* and Reed Thorkildsen*
*Department of Physics and ‡Biophysics Program, University of Virginia, Charlottesville, Virginia 22901

ABSTRACT The orientation and temperature dependence (4.2–2.5 K) of electron paramagnetic resonance (EPR) power saturation and spin-lattice relaxation rate, and the orientation dependence of signal linewidth, were measured in single crystals of the aquo complex of ferric sperm whale skeletal muscle myoglobin. The spin-packet linewidth was found to be temperature independent and to vary by a factor of seven within the heme plane. An analysis is presented which enables one to arrive at (*a*) hyperfine component linewidths and, from the in-plane angular variation of the latter, at (*b*) the widths of distributions in energy differences between low-lying electronic levels and (*c*) the angular spread in the in-plane principal *g*-directions. The values of the energy level distributions in crystals obtained from the measurements and analysis reported here are compared with those obtained by a different method for the same protein complex in frozen solution. The spread in the rhombic energy splitting is significantly greater in solution than in the crystal.

I. INTRODUCTION

Spectroscopic and relaxation measurements are providing not only energy level differences but, with appropriate experimental conditions and analysis, also widths of levels at the high-spin ferric site in myoglobin crystals (1, 2) and solutions (1, 3–6). In terms of the data available at this time, the four-level model (7–9), shown in Fig. 1, is adequate to characterize the high-spin ferric heme sites in myoglobin and hemoglobin. We report here how the orientation dependence of the linewidth of electron resonances from the heme plane of the crystals can be analyzed to obtain: σ_1 and σ_2, the rms widths of energy differences Δ_1 and Δ_2, respectively; σ_γ, the rms width of the rhombic splitting γ; and σ_ϕ, the rms angular spread in the principal x(or 2)-direction.[1] Methods employed with frozen solutions have supplied σ_1 within ±10%. From frozen solution electron paramagnetic resonance (EPR) spectra (10, 11), one can obtain $\sigma_{E/D}$, the rms width of the distribution in the rhombic to tetragonal symmetry ratio E/D. $\sigma_{E/D}$ can then be used to estimate σ_γ. Taken together, the data and analysis presented in Sections II, III, VI, and VII, below, enable one to compare the crystal and solution states of myoglobin with regard to energy level distributions at the heme site.

The phenomena just outlined are associated with inhomogeneous broadening. We are also investigating anisotropies in homogeneous broadening by means of measurements of the orientation and temperature dependence of spin-lattice relaxation time, T_1, and microwave power, P_{ms}, at the maximum EPR (first derivative) signal, in the crystal. A very large anisotropy in power saturation was found in solutions of high-spin ferric hemeproteins at 4.2 K, and an explanation was offered in terms of the product of anisotropies of transition probability, spin-lattice relaxation, and spin-packet linewidth (12). The results of the single crystal saturation/recovery study reported in Section V, below, enable one to comment quantitatively upon the temperature and orientation dependences of T_1, P_{ms}, the zero-field splitting parameter D, and the spin-packet linewidth σ.

Angular variation of the observed EPR linewidth in crystals of hemoglobin and myoglobin can be explained in terms of distributions in the directions and magnitudes of the principal *g*-values (13–15). A random misorientation of the heme normals, with a Gaussian distribution having an rms width (σ_θ) of 1.6°, was used to account for the linewidth variation in the region between the $g = 2$ direction and the $g = 6$ plane of sperm whale skeletal

Dr. Fiamingo's present address is Instruction and Research Computer Center, and Department of Physiological Chemistry, Ohio State University, Columbus, OH 43210.

Dr. Hampton's present address is Formative Technologies, Pittsburgh, PA 15213.

Dr. Thorkildsen's present address is AT&T Bell Laboratories, Murray Hill, NJ 07974.

Correspondence should be addressed to Dr. Brill.

[1]Here, the order of the *g*-values follows the convention $g_1 > g_2 > g_3$ (corresponding to the order in which resonances occur as the field is increased). Taking the principal axis belonging to g_3 to be the *z*-direction, one finds that the assignment of the *x*-and *y*-directions to the 2- and 1-principal axes orders the quantum mechanically calculated [with $S_2 = S_x = \frac{1}{2}(S_+ + S_-)$ and $L_2 = L_x = \frac{1}{2}(L_+ + L_-)$] values $g_1 > g_2$.

0006-3495/89/01/67/11 $2.00

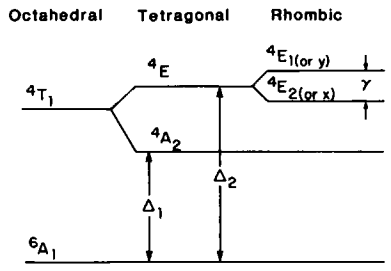

FIGURE 1 Energy level diagram of low-lying electronic states of high-spin ferric heme.

muscle myoglobin crystals (13). Employing a refinement of the latter analysis, specifically Fig. 4 of reference 16, one finds $\sigma_\theta = 1.4°$. (The disorder angle η_D of reference 15 and σ_θ are related by $\eta_D = \sqrt{2}\,\sigma_\theta$, i.e., η_D from Fig. 4 is 2.0°.) In the region between the $g = 2$ direction and the $g = 6$ plane, the g-values change rapidly with orientation so that contributions from many hemes, slightly misaligned, will generate broad lines. At the turning points of the g-values, the principal directions, these effects will be minimal and narrower lines will result. (There is, however, an interesting difference between crystals of myoglobin and hemoglobin at the $g = 2$ resonance where, for hemoglobin, the band shape is more like that from a polycrystalline sample [15]. This arises from the greater crystalline state disorder in hemoglobin, $\sigma_\theta = 2.8°$, about twice that in myoglobin crystals.)

Within the heme plane the variation in g is small, <2%, Fig. 2, but the linewidth variation can be larger, 50% at

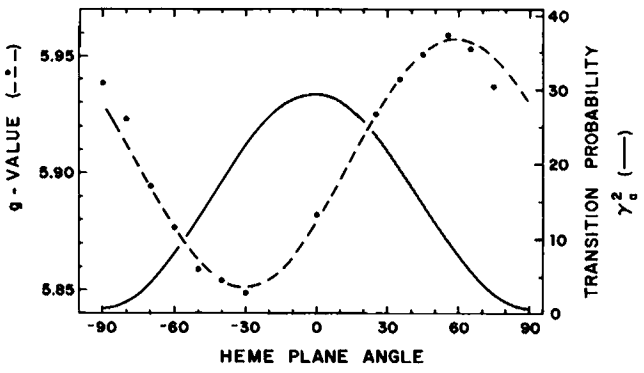

FIGURE 2 g-values and transition probability in the heme plane of a sperm whale ferric myoglobin crystal. The solid circles are the measured g-values. The dashed line is a least squares fit to these points of the function

$$g_\perp(\phi) = (g_e/2)[6-12\eta^2 - g_- \cos^2(\phi-\phi_o)],$$

where ϕ is the heme plane angle and ϕ_o marks the principal x-direction. The solid line is the calculated angular part of the transition probability, γ_a^2, in units of $(\mu_B/\hbar)^2$.

X-band (9.3 GHz) (1), and 250% at Q-band (37 GHz) (13). Helcké et al. noted that an improbably large (as lattice disorder) spread in orientation of g_x-directions within the heme plane is required to explain the Q-band data, and were of the opinion that a directional spread alone is insufficient to account for the in-plane linewidth variation (13). Calvo and Bemski showed that such variation could be explained on the basis of independently fluctuating principal directions and values of the zero-field splitting tensor (14). However, because the principal values depend in part upon the same crystal field energies, there is some correlation in the fluctuations. Therefore, in the treatment of Section III below, we formulate the microwave frequency-dependent in-plane linewidth orientation dependence in terms of fluctuations in energy differences and principal x-direction of the four-level center, including concomitant distribution in quartet state mixing (1, 2). At the end of Section III the frequency-independent contributions to the linewidth orientation dependence are treated.

A list of symbol definitions is provided in the glossary below to help the reader keep track of the notation.

GLOSSARY

Δ_1	energy difference between the $^4A_2$ and $^6A_1$ levels (Fig. 1)
Δ_2	energy difference between the ^4E and $^6A_1$ levels (Fig. 1)
γ	energy difference between the rhombically split ^4E levels, (Fig. 1)
Δ_{2x}, Δ_{2y}	energy differences between each of the rhombically split ^4E levels and the $^6A_1$ level
σ_1, σ_2	widths of energy differences Δ_1 and Δ_2
σ_γ	width of rhombic splitting energy
σ_ϕ	angular spread in principal 2-axis
D	zero-field, tetragonal, splitting energy factor
E/D	rhombic to tetragonal symmetry ratio
$\sigma_\parallel$	spin-packet linewidth, magnetic field along heme normal
$\sigma_\perp$	spin-packet linewidth, magnetic field in heme plane
$LW_{P\text{-}T}$	observed peak-to-trough resonance linewidth
LW_c	linewidth, peak-to-trough, of individual nitrogen hyperfine bands
$\eta_1, \eta_2(\eta_{2x}, \eta_{2y})$	parameters for spin-orbit mixing of excited quartet states into lowest Kramers doublet of $^6A_1$
ρ	relates (at lowest order) change in γ to

	angular displacement (in heme plane) of principal 2-axis from its average direction
λ	effective spin-orbit coupling constant
T_1	spin-lattice relaxation time
P_{ms}	microwave power at maximum EPR signal

II. IN-PLANE G-VALUES FOR HIGH-SPIN FERRIC HEME

The g-values are interpreted, following Scholes (16, 17), in terms of a second-order spin Hamiltonian for the $S = 5/2$ ferric ion,

$$\mathcal{H}_{sp} = g_e\mu_B \mathbf{B}\cdot\mathbf{S} + D[S_3^2 - S(S+1)/3] + E(S_2^2 - S_1^2) \quad (1)$$

(g_e is the free spin electronic g-value 2.0023) and refer to a fictitious spin 1/2 doublet, S':

$$g_1/2 = g_1\langle 1/2, -1/2|S_1'|1/2, +1/2\rangle = |\langle 5/2, -1/2|g_eS_1 + L_1|5/2, +1/2\rangle| \quad (2)$$

$$g_2/2 = g_2\langle 1/2, -1/2|S_2'|1/2, +1/2\rangle = |\langle 5/2, -1/2|g_eS_2 + L_2|5/2, +1/2\rangle| \quad (3)$$

The analysis of Scholes has been extended by Fiamingo (1) to include small high-order corrections arising from spin-orbit mixing of the excited quartet states into the lowest Kramers doublet. With the matrix elements from, e.g., Table 6.5 of Weissbluth (18), one finds for the lowest doublet

$$\begin{aligned}|5/2 \pm 1/2\rangle &= \sqrt{1 - (43/9)(E/D)^2 - 6\eta_1^2 - 2(\eta_{2x}^2 + \eta_{2y}^2)}\,|^6A_1 \pm 1/2\rangle \\ &- (3/\sqrt{2})(E/D)|^6A_1 \pm 3/2\rangle \\ &- (10/\sqrt{6})(E/D)|^6A_1 \pm 5/2\rangle \\ &- i\sqrt{6}\,\eta_1|^4T_{1z} \pm 1/2\rangle \mp i/\sqrt{2}\,\eta_{2x}|^4T_{1x} \pm 3/2\rangle \\ &+ (1/\sqrt{2})\,\eta_{2y}|^4T_{1y} \pm 3/2\rangle \\ &\pm i\sqrt{3/2}\,\eta_{2x}|^4T_{1x} \mp 1/2\rangle \\ &+ \sqrt{3/2}\,\eta_{2y}|^4T_{1y} \mp 1/2\rangle. \end{aligned} \quad (4)$$

The resulting in-plane g-values are

$$g_1 = g_e[3 + 12(E/D)N_{norm} - (28/3)(E/D)^2 - 6(\eta_1^2 + \eta_2^2)] - 12\eta_1\eta_2 \quad (5)$$

$$g_2 = g_e[3 - 12(E/D)N_{norm} - (28/3)(E/D)^2 - 6(\eta_1^2 + \eta_2^2)] - 12\eta_1\eta_2 \quad (6)$$

where

$$N_{norm} = \sqrt{1 - (43/9)(E/D)^2 - 6\eta_1^2 - 4\eta_2^2}, \quad (7)$$

$$\eta_1 = \lambda/\sqrt{5}\Delta_1, \quad (8)$$

$$\eta_2 = \lambda/\sqrt{5}\Delta_2, \quad \text{with } \Delta_2 = 1/2(\Delta_{2x} + \Delta_{2y}), \quad (9)$$

and

$$E/D = (\sqrt{5}\gamma/2\lambda)[\eta_2^2/(\eta_1 - \eta_2)]. \quad (10)$$

When $E = 0$, g_1 and g_2 reduce to the axial $g_\perp^{eff}$ of Eisenberger and Pershan (19) for $\gamma' = -1$.

III. FORMULATION OF EFFECTS OF ENERGY LEVEL AND DIRECTIONAL DISTRIBUTIONS UPON HYPERFINE COMPONENT LINEWIDTH

We suppose that there is a distribution in site structures giving rise to distributions in the energy level differences Δ_1, Δ_2, and γ of Fig. 1 and in the directions of the rhombic axes x (or 2) and y (or 1). For any one of these sites, the variation of g in its heme plane is, with $g_1 > g_2$ ($>g_3$),

$$g_\perp^2 = g_2^2\cos^2\phi + g_1^2\sin^2\phi = 1/2(g_1^2 + g_2^2) - 1/2(g_1^2 - g_2^2)\cos 2\phi, \quad (11)$$

where, from Section II,

$$g_{1,2} = g_e[3 \pm 12(E/D)N_{norm} - (28/3)(E/D)^2 - 6(\eta_1^2 + \eta_2^2)] - 12\eta_1\eta_2 \quad (12)$$

and $\phi = 0$ corresponds to the direction of g_x(or g_2). It is convenient, for the purpose of this analysis, to define

$$\bar{g} \equiv (1/2)(g_1 + g_2) \quad \text{and} \quad g_- \equiv g_1 - g_2. \quad (13)$$

For the aquo complex of ferric myoglobin, $\bar{g} = 5.90$, $g_- = 0.11$, and $(g_-/2\bar{g})^2 = 8.7 \times 10^{-5}$. An excellent approximation for the heme plane is then

$$g_\perp = \bar{g}[1 - (g_-/2\bar{g})\cos 2\phi] = \bar{g} - (1/2)g_-\cos 2\phi \quad (14)$$

From g_1 and g_2 above, with $12 \simeq 6g_e$, $\eta_1^2 + \eta_2^2 + \eta_1\eta_2 \gg (E/D)^2$, and $(E/D)N_{norm}$ from Section II,

$$\bar{g} = 3g_e[1 - 2(\eta_1^2 + \eta_2^2 + \eta_1\eta_2)] \quad (15)$$

and

$$g_- = 24g_e(E/D)N_{norm} = 12\sqrt{5}\,g_e\gamma\eta_2^2(1 - 3\eta_1^2 - 2\eta_2^2)/\lambda(\eta_1 - \eta_2). \quad (16)$$

For an arbitrary direction of the magnetic field, $g^2 = g_\perp^2\sin^2\theta + g_3^2\cos^2\theta$. The magnetic flux density for resonance is, with ν the microwave frequency, $B_r = h\nu/\mu_B g$. If a small fluctuation in one of the site parameters

gives rise to δg, then, to first order, the associated shift in resonance field is $\delta B_r = (-h\nu/\mu_B)\,\delta g/[\bar{g}^2 - \bar{g}g_- \cos 2\phi)\sin^2\theta + g_3^2\cos^2\theta]$. The <2% variation with ϕ in the denominator is of no consequence compared with the hyperfine component linewidth variation of almost 50%, and we neglect it in the following calculation, but this variation would have a noticeable effect in more rhombic sites. The calculation of the mean square widths of the component hyperfine lines then starts with

$$\delta B_r = (-h\nu/\mu_B)\,[\delta g/(\bar{g}^2 \sin^2\theta + g_3^2\cos^2\theta)] \qquad (17)$$

and we consider all possible sources of variation in g.

If the g-tensor of a particular site is misoriented with respect to the average g-tensor such that the deviation $\delta\theta$ of the principal g_3 (heme normal) from the average g_3 direction is small, the other two angles of the Euler angle transformation appear as their sum. In this approximation, the latter sum is well represented by $\delta\phi$, the deviation of the g_2 direction when projected upon the average heme plane. The deviation in g associated with misorientations $\delta\theta$ and $\delta\phi$ is

$$\delta g \simeq \delta\theta\frac{\partial g}{\partial\theta} + \delta\phi\frac{\partial g}{\partial\phi} + \left(\frac{1}{2}\right)\left[(\delta\theta)^2\frac{\partial^2 g}{\partial\theta^2} + 2(\delta\theta)(\delta\phi)\frac{\partial g}{\partial\theta}\frac{\partial g}{\partial\phi} + (\delta\phi)^2\frac{\partial^2 g}{\partial\phi^2}\right] \qquad (18)$$

Close to the heme plane ($\theta = 90°$) one finds

$$\delta g \simeq -(\tfrac{8}{3})(\delta\theta)^2 + g_-(\sin 2\phi)\delta\phi + \text{term in } \delta(\phi)^2, \qquad (19)$$

and, for $\delta\theta = \langle(\delta\theta)^2\rangle^{1/2} \equiv \sigma_\theta = 1.4°$, the term in $(\delta\theta)^2$ contributes negligibly ($\delta g/\bar{g} = -2.7\times10^{-4}$) to line broadening. The effects of $\delta\phi$ are included in the analysis now to be given, which also includes distributions in the site parameters η_1, η_2, and γ (where η_1 and η_2, rather than Δ_1 and Δ_2, are chosen for convenience). The in-plane linewidth, to which we now restrict our attention, is obtained from

$$\delta g_\perp = \frac{\partial\bar{g}}{\partial\eta_1}\delta\eta_1 + \frac{\partial\bar{g}}{\partial\eta_2}\delta\eta_2 - \left(\frac{1}{2}\right)g_-\left(\frac{\partial\cos 2\phi}{\partial\phi}\right)\delta\phi - \left(\frac{1}{2}\right)(\cos 2\phi)\cdot\left(\frac{\partial g_-}{\partial\eta_1}\delta\eta_1 + \frac{\partial g_-}{\partial\eta_2}\delta\eta_2 + \frac{\partial g_-}{\partial\gamma}\delta\gamma + \frac{\partial g_-}{\partial\phi}\delta\phi\right), \qquad (20)$$

where all the derivatives are evaluated at δ(parameter) = 0. Note that two terms are associated with $\delta\phi$, the first arising from a misorientation in g_2 (and g_1) not associated with a change in g_-, and the second expressing an effect of structural inhomogeneity whereby there can be a set of sites with principal axes at $\delta\phi$ and $\delta\phi + 90°$ and with rhombicity differing from the average. If one assumes that the fluctuations in η_1, η_2, γ, and ϕ are not correlated, then

$$\begin{aligned}\langle\delta g_\perp^2\rangle &= \left(\frac{\partial\bar{g}}{\partial\eta_1} - \frac{\cos 2\phi}{2}\frac{\partial g_-}{\partial\eta_1}\right)^2\langle\delta\eta_1^2\rangle + \left(\frac{\partial\bar{g}}{\partial\eta_2} - \frac{\cos 2\phi}{2}\frac{\partial g_-}{\partial\eta_2}\right)^2\langle\delta\eta_2^2\rangle \\ &+ \left(-\frac{\cos 2\phi}{2}\frac{\partial g_-}{\partial\gamma}\right)^2\langle\delta\gamma^2\rangle + \left(-\frac{\cos 2\phi}{2}\frac{\partial g_-}{\partial\phi} + g_-\sin 2\phi\right)^2\langle\delta\phi^2\rangle \\ &= (3g_e)^2\,[L + M\cos 2\phi + N\cos(4\phi - \beta_N)] \qquad (21)\end{aligned}$$

where

$$L \equiv (3g_e)^{-2}\{(a^2 + \tfrac{1}{2}b^2)\langle\delta\eta_1^2\rangle + (c^2 + \tfrac{1}{2}d^2)\langle\delta\eta_2^2\rangle + \tfrac{1}{2}f^2\langle\delta\gamma^2\rangle + \tfrac{1}{2}(f^2\rho^2 + g_-^2)\langle\delta\phi^2\rangle\}, \qquad (22)$$

$$M \equiv 2(3g_e)^{-2}(ab\langle\delta\eta_1^2\rangle + cd\langle\delta\eta_2^2\rangle), \qquad (23)$$

$$N^2 \equiv (3g_e)^{-4}\{\tfrac{1}{4}[b^2\langle\delta\eta_1^2\rangle + d^2\langle\delta\eta_2^2\rangle + f^2\langle\delta\gamma^2\rangle + (f^2\rho^2 - g_-^2)\langle\delta\phi^2\rangle]^2 + [f\rho g_-\langle\delta\phi^2\rangle]^2\}, \qquad (24)$$

and

$$\tan\beta_N \equiv 2f\rho g_-\langle\delta\phi^2\rangle/[b^2\langle\delta\eta_1^2\rangle + d^2\langle\delta\eta_2^2\rangle + f^2\langle\delta\gamma^2\rangle + (f^2\rho^2 - g_-^2)\langle\delta\phi^2\rangle], \qquad (25)$$

with

$$a \equiv \partial\bar{g}/\partial\eta_1, \quad b \equiv -\tfrac{1}{2}\partial g_-/\partial\eta_1, \quad c \equiv \partial\bar{g}/\partial\eta_2, \quad d \equiv -\tfrac{1}{2}\partial g_-/\partial\eta_2, \quad f \equiv -\tfrac{1}{2}\partial g_-/\partial\gamma, \quad \text{and } \rho \equiv \partial\gamma/\partial\phi. \qquad (26)$$

Formulas for a, b, c, d, and f, expressed in terms of η_1, η_2, and γ are readily obtained (e.g., $a/6g_e = -2\eta_1 - \eta_2$) and η_1, η_2, and γ are calculable from the measured values of g_1, g_2, and the zero-field splitting D (see below). The range of the parameter ρ will be shown to be constrained by the linewidth variation data. An interesting feature of the angular variation of the linewidth is the dependence of the phase factor β_N upon the fluctuations in the energy ($\delta\eta_i$) and orientation ($\delta\phi$) parameters. Because β_N is obtained from the data, the mean square fluctuations are related experimentally through, e.g., the formula for $\tan\beta_N$. It is therefore possible to express $\langle\delta\phi^2\rangle$ in terms of the $\langle\delta\eta_i^2\rangle$, as follows:

$$\langle\delta\phi^2\rangle = P(b^2\langle\delta\eta_1^2\rangle + d^2\langle\delta\eta_2^2\rangle + f^2\langle\delta\gamma^2\rangle) \qquad (27)$$

where

$$P \equiv \tan\beta_N/[2f\rho g_- + (g_-^2 - f^2\rho^2)\tan\beta_N]. \qquad (28)$$

In terms of P, the positive root of N^2 is

$$N = \tfrac{1}{2}\{(1 + \tan^2\beta_N)^{1/2}[1 + (f^2\rho^2 - g_-^2)P]\}\cdot[b^2\langle\delta\eta_1^2\rangle + d^2\langle\delta\eta_2^2\rangle + f^2\langle\delta\gamma^2\rangle]. \qquad (29)$$

One then has three linear algebraic equations in the unknowns $\langle \delta\eta_1^2 \rangle$, $\langle \delta\eta_2^2 \rangle$, and $\langle \delta\gamma^2 \rangle$:

$$\begin{aligned} l_1\langle \delta\eta_1^2 \rangle + l_2\langle \delta\eta_2^2 \rangle + l_3\langle \delta\gamma^2 \rangle &= L \\ m_1\langle \delta\eta_1^2 \rangle + m_2\langle \delta\eta_2^2 \rangle + m_3\langle \delta\gamma^2 \rangle &= M \\ n_1\langle \delta\eta_1^2 \rangle + n_2\langle \delta\eta_2^2 \rangle + n_3\langle \delta\gamma^2 \rangle &= N. \end{aligned} \tag{30}$$

Here

$$\begin{aligned} l_1 &= a^2 + [(f^2\rho^2 + g_-^2)P + 1](b^2/2) \\ l_2 &= c^2 + [(f^2\rho^2 + g_-^2)P + 1](d^2/2) \\ l_3 &= [(f^2\rho^2 + g_-^2)](f^2/2) \\ m_1 &= 2ab, \quad m_2 = 2cd, \quad m_3 = 0 \end{aligned} \tag{32}$$

$$\begin{aligned} n_1 &= \{\tfrac{1}{2}(1 + \tan^2\beta_N)^{1/2}[1 + (f^2\rho^2 - g_-^2)P]\}b^2 \\ n_2 &= \{\tfrac{1}{2}(1 + \tan^2\beta_N)^{1/2}[1 + (f^2\rho^2 - g_-^2)P]\}d^2 \\ n_3 &= \{\tfrac{1}{2}(1 + \tan^2\beta_N)^{1/2}[1 + (f^2\rho^2 - g_-^2)P]\}f^2. \end{aligned} \tag{33}$$

For a set of experimentally determined values of L, M, and N, the system of equations does not have a unique solution because the parameter ρ is unknown. Rather, in the calculation, ρ is systematically varied. Valid solutions and the range of allowed ρ are determined by the requirement $\sigma_i^2 \geq 0$.

In starting the analysis for obtaining L, M, and N from the experimental data, we denote by δB_O those contributions to the hyperfine component linewidth which do not arise from a distribution in g-tensors, and hence are frequency independent. The mean square linewidth (one-half peak-to-trough) in the heme plane is

$$\begin{aligned} (LW_c/2)^2 &= \langle \delta B_O^2 \rangle + \langle \delta B_r^2 \rangle \\ &= \langle \delta B_O^2 \rangle + \langle h\nu/\mu_B\bar{g}^2 \rangle^2 \langle \delta g_\perp^2 \rangle \\ &= L_O + M_O \cos 2(\phi - \alpha) + N_O \cos(4\phi - \beta), \end{aligned} \tag{34}$$

where $\phi = 0$ is the g_x-direction, and L_O, M_O, N_O, and β are determined experimentally as in Fig. 6. The frequency-independent contributions arise from the dipolar broadening interactions of each ferric ion with other ferric ions; with proton dipoles on the protein, the prosthetic group, and water molecules; and with other paramagnetic nuclei. In both parts of the Van Vleck formula for dipolar broadening, there are trigonometric factors $(1 - 3 \cdot \cos^2\theta_{jk})^2$ where θ_{jk} is the angle between the applied magnetic field and the radius vector from ferric ion j to dipole k. It can readily be shown that the contributions to the mean square spread in resonant frequency from dipoles with isotropic g-values are of the form

$$A + B\cos 2(\phi - \phi_{jk}) + C\cos 4(\phi - \phi_{jk}),$$

where ϕ is the direction of the applied field within the heme plane and ϕ_{jk} is a phase factor. While the nuclear g-values are isotropic, the ferric tensor is highly anisotropic. However, for the geometry under consideration, the effect of this anisotropy is small; the heme normals in the sperm whale myoglobin crystal are at 43° and, as **B** is rotated around the heme plane of one site, g at the other site ranges from 4.5 to 5.9 (i.e., 5.2 ± 13%). To a good approximation, then, the sum of the frequency-independent contributions to the mean square linewidth is

$$\langle \delta B_o^2 \rangle = A + B\cos 2(\phi - \phi_B) + C\cos 4(\phi - \phi_c) \tag{35}$$

and

$$\begin{aligned} (LW_c/2)^2 &= L_o + M_o\cos 2(\phi - \alpha) + N_o\cos(4\phi - \beta) \\ &= A + B\cos 2(\phi - \phi_B) + C\cos 4(\phi - \phi_C) \\ &\quad + \left(\frac{3g_e h\nu}{\mu_B\bar{g}^2}\right)^2 [L + M\cos 2\phi + N\cos(4\phi - \beta_N)] \end{aligned} \tag{36}$$

IV. MATERIALS AND METHODS

Myoglobin crystals

Lyophilized protein was obtained commercially. The powder was dissolved in slightly alkaline 6 mM ferricyanide in 5 mM PO_4. After adjustment of pH to 6.2 with acid phosphate buffer, the solution was poured onto a carboxymethyl cellulose column, and the column then washed with 10 mM PO_4, pH 6.3. Free metal ions were removed by passing 5 mM EDTA (pH adjusted to 6.3) through the column. The solution eluted from the column contained myoglobin at a concentration of ~1 mM. The protein was then dialyzed against 33 mM PO_4, pH 6.33; centrifuged to remove denatured protein; concentrated by dialysis against saturated ammonium sulfate; redialyzed against 33 mM PO_4, and recentrifuged. Crystals were prepared by a method similar to that of Kendrew and Parrish (20). 100 μl of ~7 mM myoglobin was added to 1 ml of saturated ammonium sulfate brought to pH 5.8 with Na_2H PO_4. The largest crystals were grown from a solution on the verge of losing clarity (becoming overconcentrated). Crystals formed overnight at room temperature, the largest being about 0.7 × 0.7 × 1.5 mm^3. Sperm whale skeletal muscle myoglobin Type A crystals belong to the monoclinic space group $P2_1$ with two molecules per unit cell. The two $g = 2$ (g_3) directions are 43° apart (positive and negative directions are indistinguishable).

EPR measurements

Single crystal EPR spectra, at temperatures in the range 2.5–4.2 K, were taken with the apparatus described in reference 15, modified in its microwave bridge. Power from the klystron is split, with one part going first to the cavity and then to the detector, and the other part going directly to the detector to provide continuous bias. The bias arm has an attenuator for power control, and a phase shifter to bring the bias wave into coherence with the wave from the cavity arm at the detector. The cavity arm has an attenuator, circulator, termination, and a pair of matched 30-db microwave switches (Microwave Associates, Inc., Burlington, MA; 8319-1X9.35) for use in spin-lattice relaxation measurements. For the latter, the method of Isaacson (21) was employed, with a

160 boxcar integrator (Princeton Applied Research, Princeton, NJ) and 400-Hz field modulation. T_1 values were obtained from nonlinear least squares fits of an exponential function to the saturation recovery curves.

Microwave field measurement in the cavity

To determine the microwave magnetic flux density B_1 in the EPR cavity, the method of perturbing spheres formulated by Maier and Slater (22) was used. Here the shift $\nu - \nu_o$ in the resonant frequency of the cavity caused by the introduction of a metallized sphere of radius r_o is related to the mean square value of B_1 in Gauss (all else in SI units) by

$$B_1^2 = \frac{P\mu_o}{2\pi^2 r_o^3}\left(\frac{\nu - \nu_o}{\Delta\nu}\right)\left(\frac{1}{\nu_o}\right) \times 10^8, \qquad (37)$$

where P is the power incident upon the cavity, $\Delta\nu$ is the full width at half maximum of the power reflected from the cavity at total reflection, and μ_o is the permeability of free space. Nonmagnetic spheres of radii in the range 0.6–1 mm were made from soft glass rod, and a conducting surface applied by firing "Liquid Bright Gold" (Engelhard Ind., Inc., East Newark, NJ) onto the glass four times. One of these spheres was then held rigidly with styrofoam inside a quartz tube; the shift in resonant frequency upon insertion of the tube in the cavity, and the width of the cavity resonance, could both be measured directly (in mm) from an oscilloscope mode display. Six such spheres out of seven gave the same result within 5%. Correction for microwave absorption by the protein crystal is not included. (It should be noted that knowledge of the actual value of B_1^2 is not necessary for the analysis given in the following section [V] because D is obtained from the temperature dependence of ln $[P_{ms}]$. However, this knowledge provides quantitatively the range of P_{ms} values given by the left ordinate of Fig. 3.)

V. TEMPERATURE AND ORIENTATION DEPENDENCE OF POWER SATURATION AND SATURATION RECOVERY

Measurements for the purpose of determining the principal g-tensor directions were made on one crystal, giving the directions with respect to the a, b, and c^* crystal axes shown in Table 1. The heme normal directions differ little from those reported previously from EPR measurements (23, 24) and from x-ray diffraction (25). The orientations of other crystals used in our experiments may differ from this one by a few degrees due to misalignment of the crystals relative to the laboratory reference.

A survey of the orientation dependence of spin-lattice relaxation and power saturation was carried out. In the temperature range (4.2–2.5 K) of the measurements reported here, with the zero-field separation $2D$ (of the $m_s = \pm 3/2$ spin levels from the ground $m_s = \pm 1/2$ levels; with $D = 8$ cm^{-1}, the $m_s = \pm 5/2$ levels are expected to contribute less than 0.1% to the relaxation at 4.2 K) in the range 10 to 20 cm^{-1}, the dominant relaxation mechanism is expected to be a two-phonon Orbach process, with the direct process becoming more important as the temperature decreases. If the Orbach process were solely responsible for spin-lattice relaxation, and there were negligible spread in D, then the temperature dependence of the characteristic time would be

$$1/T_1 = A \exp(-2D/k_B T). \qquad (38)$$

Measurements of the temperature dependence of saturation recovery kinetics in frozen solutions of the aquo complexes of ferric myoglobins show an almost linear region between 4.2 and 2.8 K in plots of ln $(1/T_1)$ vs. $1/T$, with curvature developing in these plots at lower temperatures (3–6). These data from solutions at cryogenic temperatures have been the subject of a detailed analysis, involving consideration of the distributions in D arising from distributions in the energies of the lowest electronic levels (4–6). The system average of D for myoglobin in frozen solution exceeds by 6 to 8% the value obtained by a linear least squares fit to ln $(1/T_1)$ vs. $1/T$ between 3.71 and 2.86 K; the factor 1.07 will be used below in estimating the average D from the slope in the linear region. It will be a major undertaking to collect, from single crystals at many orientations, saturation recovery kinetic data at the large number of temperatures and with the precision of these recent frozen solution measurements. The temperature dependence of T_1 and P_{ms} reported below is from data taken at four to six points in the temperature range studied.

Before taking up the single crystal investigations, we augmented early power saturation studies on solutions at 4.2 K with measurements of the temperature dependence of both the microwave power at the maximum signal, P_{ms}, and the spin-lattice relaxation time, T_1 (which, in the analysis employed here, characterizes the best fit to a single exponential). (Recall that, for the protein frozen in solution, a $g = 2$ signal is observed from those molecules oriented with their heme plane normal along the direction of the scanning magnetic field, while those oriented perpendicular to this direction exhibit a $g = 6$ signal. This $g = 6$ signal in frozen solution then represents the weighted average of many orientations within and near the heme plane.) For the $g = 2$ and $g = 6$ resonances separately, we found that T_1 and P_{ms} vary inversely with respect to each other such that the product $T_1 P_{ms}$ remains constant (within experimental uncertainty) when the temperature is changed. This observation can be

TABLE 1 Directions of principal g-values with respect to crystal axes

	a	b	c^*
g_1	93.8	119.4	29.7
g_2	121.5	40.4	67.4
g_3	32.0	64.5	72.0

expressed in terms of the zero-field splitting parameters D obtained separately from the dependences of ln $(1/T_1)$ and ln (P_{ms}) upon reciprocal temperature. Table 2a gives average values from measurements on two solutions. (The overall average of these D-values, 8.4 cm^{-1}, differs by 6% from the value 7.9(3) cm^{-1} obtained in experiments of greater precision designed for characterizing energy level distributions in hemeprotein solutions [4–6]). The constancy of the T_1P_{ms} product indicates that the spin-packet linewidth σ is independent of the temperature in this range. It has been shown that $\sigma \propto \gamma_a^2 T_1 P_{ms}$, where γ_a^2 is the angular part of the transition probability (12). This term depends upon the orientations of the scanning field **B** and the microwave field $\mathbf{B}_1$ (taken perpendicular to **B**) with respect to the principal g-directions, and reduces to

$$\gamma_i^2 = (\mu_{B^2}/2\hbar^2)(g_j^2 + g_k^2) \tag{39}$$

for a frozen solution. (P_{ms} is proportional to $\mathbf{B}_1^2$ at maximum signal.) Then the ratio of spin-packet linewidths perpendicular and parallel to the heme normal is

$$\sigma_\perp/\sigma_\parallel = [(g_\perp^2 + g_\parallel^2)/2g_\perp^2](T_1P_{ms})_\perp/(T_1P_{ms})_\parallel. \tag{40}$$

We find $\sigma_\perp/\sigma_\parallel = 2.26$ for the frozen solution of the aquo complex of ferric sperm whale skeletal myoglobin.

The temperature dependences of T_1 and P_{ms} were measured on two crystals, with **B** along the heme normal and at three orientations within the heme plane. Table 2b gives average values of D estimated from this data. (The overall average, 8.0 cm^{-1}, of these D-values weighted according to number of orientations, differs little from the 7.9(3) value from precise solution measurements.) At each orientation, the product T_1P_{ms} was found to be independent of temperature and the D-values from the temperature dependences of T_1 and P_{ms} were found to be the same, within experimental uncertainty. This behavior is shown in Fig. 3 which displays data taken at an orientation in the heme plane where $g = 5.94$.

TABLE 2 Average values of the zero-field splitting parameter D

Measurement condition	D from $T_1(T)$	D from $P_{ms}(T)$
	cm^{-1}	cm^{-1}
a. From measurements on two solutions		
$g = 2.00$	8.5	7.4
$g = 5.86$	8.8	8.8
b. From measurements on two crystals, with **B** along the heme normal and at three orientations within the heme plane.		
B along heme normal	8.0	8.4
B in heme plane	8.3	7.6

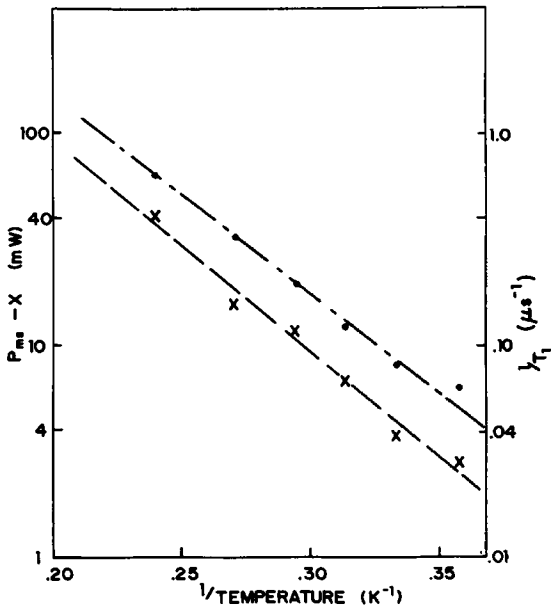

FIGURE 3 The power at maximum signal, P_{ms}, and the spin-lattice relaxation rate, $1/T_1$, are graphed, on a semi-log plot, as functions of the inverse temperature.

Measurements, at constant temperature, taken at 10° increments between the heme normal and the heme plane, and around the heme plane, show that T_1 varies by a maximum factor of 5 between the $g = 2$ and $g = 6$ directions, and by a factor of 3 within the heme plane. (In view of the large differences in concentration of protein between the solutions and crystals, it is interesting to note that, at a given temperature, the crystal heme plane average T_1 differs from the $g = 6$ solution value by only ~15%.) T_1 is a maximum in the heme plane along the N_1-N_2 (numbering scheme is that of Takano [25]) direction, as is $\gamma_a^2 P_{ms}$, so that $\sigma_\perp$ also peaks along this direction. A theoretical analysis predicted that the spin-packet linewidth would be at a maximum within the heme plane halfway between the Fe-N bond directions (26). We observe this along the N_1-N_2 direction. Along the N_2-N_3 direction the microwave magnetic field was nearly parallel to the scanning field, resulting in a low transition probability and very noisy data. However, there did not appear to be a maximum here for the spin-packet linewidth. $\sigma_\perp/\sigma_\parallel$ varied from 0.9 to 6.6 within the heme plane.

The observed peak-to-trough resonance linewidth $LW_{P\text{-}T}$ (at low power) is a maximum along the Fe-N bond directions, and a minimum halfway in between (along the maximum spin-packet linewidth orientation). The minimum in-plane g-value is within a few degrees of the x-ray diffraction-determined projection of the histidine ring

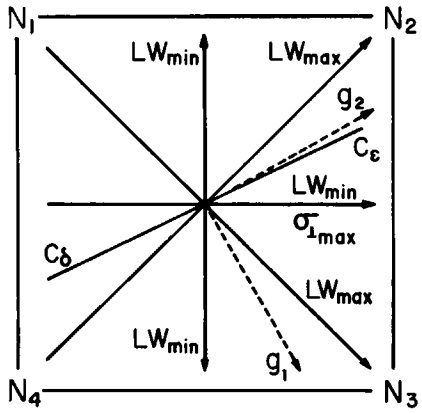

FUGURE 4 The projection of the imidazole ring of the proximal histidine, HisF8(C_α), onto the average plane of the heme nitrogens (N_i) is shown (25), as are extrema directions from the EPR data. LW is the observed peak-to-trough linewidth, and $\sigma_{\perp max}$ the maximum spin-packet linewidth, within the heme plane. The C_δ-C_ϵ projection is 19° from the N_4-N_2 direction (25). g_2 was found to be 14.5° from the N_4-N_2 direction.

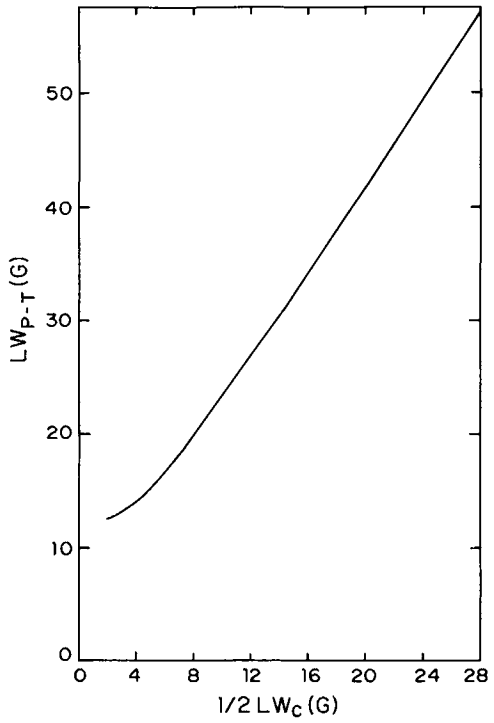

FIGURE 5 Peak-to-trough linewidth $LW_{P\text{-}T}$ of the calculated envelope of unresolved nitrogen hyperfine bands plotted as a function of the one-half peak-to-trough linewidth $\frac{1}{2}LW_c$ of the hyperfine components. The contact terms are $A_H/2\mu_B$ = 2.84 G for the heme nitrogens and $A_I/2\mu_B$ = 3.32 G for the iron-linked imidazole nitrogen of HisF8. The Scholes correction factors are $F_H/2\mu_B$ = 0.15 G and $F_I/2\mu_B$ = 0.40 G. The hyperfine separations are ΔB_H = 3.04 G and ΔB_I = 2.60 G.

onto the heme plane (25). These relations are illustrated in Fig. 4.

VI. HYPERFINE COMPONENT LINEWIDTH VARIATION

While the individual nitrogen hyperfine bands are not resolved at any orientation, the linewidths of these components can be obtained from simulations of the observed spectra (15). In this calculation, the values used for the Fermi contact terms are $A_H = 2.65 \times 10^{-4}$ cm^{-1} for the nitrogens of the heme plane, and $A_I = 3.11 \times 10^{-4}$ cm^{-1} for the iron-linked imidazole nitrogen of the proximal histidine, information available from single crystal ENDOR measurements (27). The Scholes correction factors (16) were taken as $F_H = 0.14 \times 10^{-4}$ cm^{-1} and $F_I = 0.37 \times 10^{-4}$ cm^{-1} for the heme and imidazole nitrogens, respectively. The separations used for the hyperfine lines were ΔB_H = 3.04 G and ΔB_I = 2.60 G. A plot of $LW_{P\text{-}T}$ as a function of $\frac{1}{2}LW_c$ is shown in Fig. 5. Component linewidths above about 50 G ($\frac{1}{2}LW_c \simeq 25$ G) produce envelopes of the same linewidth. The solid circles in Fig. 6 are the $LW_{P\text{-}T}$, converted to the LW_c by means of Fig. 5, and then squared.

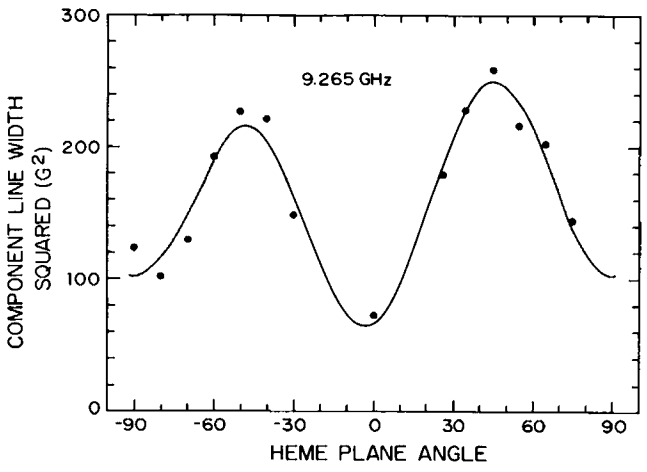

FIGURE 6 The square of the component linewidth (one-half peak-to-peak), $(\frac{1}{2}LW_c)^2$, is plotted as a function of the heme plane angle. The solid circles are the observed peak-to-trough linewidths, converted to component linewidths through the use of Fig. 5, and then squared. The line is the least squares fit to the equation

$$(\tfrac{1}{2}LW_c)^2 = L_o + M_o \cos 2(\phi - \phi_o - \alpha) + N_o \cos [4(\phi - \phi_o) - \beta],$$

where ϕ is the experimental heme plane angle and $\phi_o = -30.5°$ corresponds to the x-direction as determined by the least squares fit to the in-plane g-values, Fig. 2. L_o, 158.3; M_o, −25.0; N_o, −73.6; α, 9.1°; β, 121.5°.

VII. EXPERIMENTAL QUANTIFICATION OF ENERGY LEVEL AND DIRECTIONAL DISTRIBUTIONS

The parameters obtained from nonlinear least squares fits to the data are given in Table 3. From these one obtains the frequency-independent parameters

$$A = 71\ G^2$$
$$B = -15\ G^2, \quad \phi_B = 16°$$
$$C = 22\ G^2, \quad \phi_c = -6°$$
$$L = 6.8 \times 10^{-5}$$
$$M = -8.6 \times 10^{-6}$$
$$N = -4.4 \times 10^{-5}, \quad \beta_N = 108.5°. \qquad (41)$$

$\sqrt{A} = 8.4$ G is somewhat greater than one expects for a system like this (28). However A, which is calculated as the difference between numbers which differ from each other only by a factor of 2 and which separately have experimental errors of 10%, is uncertain to ±30%.

The values of L, M, and N can be used to constrain the rms widths σ_1, σ_2, and σ_γ of the energy differences Δ_1, Δ_2, and γ of Fig. 1 once these energies are obtained. With $\lambda = 350\ cm^{-1}$ and $D = 8.0\ cm^{-1}$ (from references 5, 6 and Section V above),

$$\Delta_1 = 2{,}040\ cm^{-1}$$
$$\Delta_2 = 6{,}140\ cm^{-1}$$
$$\gamma = 57.5\ cm^{-1} \qquad (42)$$

We then find, from solving the system of three equations given in the preceding section, the parameters given in Table 4. Solutions exist only for ρ in the range shown, from 106 to 130 cm^{-1}/rad. It is not realistic to permit $\sigma_2 < \sigma_1$; more vibrational modes affect[2] the energy difference Δ_2 than Δ_1 (3). If one conservatively defines an effective minimum $\sigma_1)_{min,eff}$ from the case where $\sigma_2 = \sigma_1 = \sigma_1)_{min,eff}$, then the parameters are $\sigma_1)_{min,eff} = 221\ cm^{-1}$ and $\sigma_\gamma = 35.1\ cm^{-1}$ with $\rho = 107\ cm^{-1}$/rad. Apart from this consideration, the allowed ranges are

$$220\ cm^{-1} < \sigma_1 < 300\ cm^{-1}$$
$$0 < \sigma_2 < 990\ cm^{-1}$$
$$0\ cm^{-1} < \sigma_\gamma < 36\ cm^{-1}$$
$$0.33\ rad\ (19°) < \sigma_\phi < 0.37\ rad\ (21°)$$
$$106\ cm^{-1}/rad < \rho < 130\ cm^{-1}/rad. \qquad (43)$$

[2]We assume here that the spread in energy (associated with a frozen in protein conformational distribution) of a particular heme state depends upon the number of normal modes which affect the energy of that state.

TABLE 3 Parameters characterizing heme plane angular dependence of hyperfine component linewidth

ν	9.265 GHz	37.48 GHz*
L_0	158 G^2	$1.52 \times 10^3\ G^2$
M_0	$-25\ G^2$	$-195\ G^2$
N_0	$-74\ G^2$	$-960\ G^2$
α	9°	~0
β	121.5°	109.5°

*Reference 14.

The energy differences and allowed ranges differ somewhat from the original estimates (2) because of small changes (based upon later experimental data) in the parameters used in their calculation, and because allowance has now been made for frequency-independent contributions to the angular dependent components of the linewidth.

VIII. DISCUSSION

At this time we are able to compare the spread σ_1 in energy of the lowest lying electronic level of the aquo complex of ferric myoglobin in the crystal with that in solution. Based upon an analysis of hyperfine component linewidth angular variation, the investigation reported here gives σ_1 in the crystal to be in the range 220 to 300 cm^{-1}. Based upon an analysis of the distribution in spin-lattice relaxation rates and hence in D, measurements on the same complex in solution gave σ_1 in the range 230 to 290 cm^{-1} (4–6). Clearly these independent methods show that there is little or no difference between crystal and solution in the width of this energy distribution. It will be useful to investigate whether or not the method involving characterization of the distribution in D to obtain σ_1, thus far applied only to the aquo complex of ferric myoglobin in solution, will, when applied to single crystals, yield a range for σ_1 in agreement with those at hand.

At this time we are also able to compare the spread $\sigma_{\gamma,s}$ in the rhombic splitting γ obtained from measurements

TABLE 4 Widths of electronic energy differences and spread in principal 2-direction

	Minimum	Corresponding ρ	Maximum	Corresponding ρ
σ_1	216 cm^{-1}	106 cm^{-1}/rad	297 cm^{-1}	130 cm^{-1}/rad
σ_2	0	106	988 cm^{-1}	130
σ_γ	0 cm^{-1}	130	36.1 cm^{-1}	106
σ_ϕ	0.333 rad	130	0.369 rad	106

on solutions with a related quantity, $\sigma_{\gamma,c}$, which can be calculated from three of the parameters given in this paper. The total spread in γ is viewed, in the first order approximation, as arising from two independent fluctuations, one in which fluctuation in γ is not accompanied by change in the principal g-directions, and the other in which fluctuation in γ is associated with change in the (in-plane) principal g-directions. One can then write

$$\sigma_{\gamma,\text{total}} = (\sigma_\gamma^2 + \rho^2\sigma_\phi^2)^{1/2}. \quad (44)$$

$\sigma_{\gamma,s} = 98\ \text{cm}^{-1}$, obtained from solution measurements (1, 3, 4, 6), is a $\sigma_{\gamma,\text{total}}$. From the analysis of the single crystal measurements, one obtains concomitantly $\sigma_{\gamma,c} = \sigma_{\gamma,\text{total}}(\rho)$; the minimum and maximum values of $\sigma_{\gamma,c}$ occur in conjunction with the parameters given in Table 5. The allowed range of $\sigma_{\gamma,c}$ is seen to be between 43 and 53 cm^{-1}. Clearly $\sigma_{\gamma,\text{total}}$ is significantly smaller for the protein in the crystal than in solution.

In the aquo complex of myoglobin, interaction of the ferric ion with the imidazole of the proximal histidine is likely to influence the in-plane principal g-directions. If distribution in orientation of this imidazole ring is associated with the spread in ϕ of ~20°, then the question arises as to the compatibility of such a structural distribution with resolution of the structure from x-ray diffraction. An rms 20° rotation of the imidazole plane about the N(ε)-Fe bond corresponds to an average mean square displacement of ~0.1 A^2 at the other ring atoms, consistent with resolution of the side chain. However, one need not attribute σ_ϕ solely to distributions in orientation of neighboring groups; for example, deviations in length of the F alpha helix (29) could modulate the interaction (of the proximal histidine with the ferric ion) which influences the principal g-directions. Also, one should recall that angular distributions obtained from measurements like those on single crystals reported here include effects of lattice disorder as well as molecular structural heterogeneity.

The constancy of the T_1P_{ms} product over the temperature range in which ln $(1/T_1)$ and ln (P_{ms}) are approximately linear functions of $1/T$ indicates that, for the aquo complex of ferric myoglobin, the spin-packet linewidth σ is independent of temperature in this range. Therefore, determination of the temperature dependence of P_{ms}, a continuous wave measurement, may enable one to approximate the zero-field splitting parameter D in related hemeprotein complexes. Hoewver, without information about the distribution of D in complexes being studied for the first time, there is a quantitative uncertainty in such an estimate, particularly when there is no curvature-free region of ln (P_{ms}) vs. $1/T$. Parameters other than P_{ms} can be used to characterize power saturation behavior; measurement of the temperature dependence of the microwave power at which the saturation factor is 0.5 has been employed to estimate D-values of high-spin metalloproteins (30).

TABLE 5 Parameters associated with spread in rhombic splitting energy in the crystal

ρ	σ_ϕ	σ_γ	$\sigma_{\gamma,\text{total}}$
130.3 cm^{-1}/rad	0.333 rad	0 cm^{-1}	43.4 cm^{-1}
105.8	0.369	36.1	53.2

The authors thank Dr. Paul D. Levin for helpful comments on the manuscript.

The support of the National Science Foundation under Grants PCM-7904361, PCM-8104377, and DMB-8517819 is acknowledged with appreciation.

Received for publication 20 May 1988 and in final form 22 September 1988.

REFERENCES

1. Fiamingo, F. G. 1980. Electron Paramagnetic Resonance Absorption and Relaxation in Heme Systems at Low Temperatures. Ph.D. dissertation, University of Virginia.
2. Fiamingo, F. G., R. Thorkildsen, and A. S. Brill. 1980. Structural distribution and rotational disorder in myoglobin crystals. *Biophys. J.* 32:634–635.
3. Thorkildsen, R. 1981. Spin Lattice Relaxation in High-Spin Ferric Hemeprotein Frozen Solutions. Ph.D. thesis, University of Virginia.
4. Levin, P. D. 1984. EPR Power Saturation Recovery in High-Spin Ferric Heme Systems: Measuring and Modeling the Effects of Energy Level Distributions. Ph.D. thesis, University of Virginia.
5. Brill, A. S., F. G. Fiamingo, D. A. Hampton, P. D. Levin, and R. Thorkildsen. 1985. Density of low-energy vibrational states in a protein solution. *Phys. Rev. Lett.* 54:1864–1867.
6. Levin, P. D, and A. S. Brill. 1988. Analysis of EPR pulse saturation recovery kinetics of myoglobin solutions. *J. Phys. Chem.* 92:5103–5110.
7. Griffith, J. S. 1956. On the magnetic properties of some haemoglobin complexes. *Proc. R. Soc. Lond. A. Math. Phys. Sci.* 235:23–36.
8. Kotani, M. 1968. Paramagnetic properties and electronic structure of iron in heme proteins. *Adv. Quantum Chem.* 4:227–266.
9. Harris, G. 1968. Zero-field splitting, magnetic-field energies, effective magnetic moments, and electric-field gradients in high-spin ferric porphyrin compounds. *J. Chem. Phys.* 48:2191–2214.
10. Brill, A. S., F. G. Fiamingo, and D. A. Hampton. 1978. Characterization of high-spin ferric states in heme proteins. *In* Frontiers of Biological Energetics. P. L. Dutton, J. S. Leigh, and A. Scarpa, editors. Academic Press, New York. 1025–1033.
11. Brill, A. S., F. G. Fiamingo, and D. A. Hampton. 1986. EPR characterization of alcohol complexes of ferric myoglobin and hemoglobin. *J. Inorg. Biochem.* 28:137–143.
12. Brill, A. S., C.-I. Shyr, and T. C. Walker. 1975. Power saturation of

electron paramagnetic resonances from high-spin ferric haemproteins at 4.2 K. *Mol. Phys.* 29:437–454.

13. Helcké, G. A., D. J. E. Ingram, and E. F. Slade. 1968. Electron resonance studies of haemoglobin derivatives. III. Line-width and g-value measurements of acid-met myoglobin and of met myoglobin azide derivatives. *Proc. R. Soc. Lond. B. Biol. Sci.* 169:275–288.
14. Calvo, R., and G. Bemski. 1976. On the electron spin resonance linewidths of met-myoglobin. *J. Chem. Phys.* 64:2264–2265.
15. Hampton, D. A., and A. S. Brill. 1979. Crystalline state disorder and hyperfine component line widths in ferric hemoglobin chains. *Biophys. J.* 25:301–312.
16. Scholes, C. P. 1970. EPR studies on heme oriented in an organic crystalline environment. *J. Chem. Phys.* 52:4890–4895.
17. Scholes, C. P. 1969. Heme Oriented in an Organic Crystalline Environment. Ph.D. dissertation, Yale University.
18. Weissbluth, M. 1974. Hemoglobin: Cooperativity and Electronic Properties. Springer-Verlag KG, Berlin, W. Germany. 110.
19. Eisenberger, P., and P. S. Pershan. 1966. Electron spin resonance of met-myoglobin: field dependence of $g_{\perp}^{\text{eff}}$. *J. Chem. Phys.* 45:2832–2835.
20. Kendrew, J. C., and R. G. Parrish. 1956. The crystal structure of myoglobin. III. Sperm whale myoglobin. *Proc. R. Soc. Lond. A. Math. Phys. Sci.* 238:305–324.
21. Isaacson, R. 1968. Use of field modulation with boxcar integrator to measure relaxation time in electron spin resonance experiments. *J. Sci. Instr. Ser.* 2, 1:1137–1139.
22. Maier, L. C., Jr., and J. C. Slater. 1952. Field strength measurements in resonant cavities. *J. Appl. Phys.* 23:68–77.
23. Bennett, J. E., J. F. Gibson, and D. J. E. Ingram. 1957. Electron-resonance studies of haemoglobin derivatives. I. Haem-plane orientation. *Proc. R. Soc. Lond. A. Math. Phys. Sci.* 240:67–82.
24. Hori, H. 1971. Analysis of the principal g-tensors in single crystals of ferrimyoglobin complexes. *Biochim. Biophys. Acta.* 251:227–235.
25. Takano, T. 1977. Structure of myoglobin refined at 2.0 Å resolution. I. Crystallographic refinement of metmyoglobin from sperm whale. *J. Mol. Biol.* 110:537–568.
26. Brill, A. S. 1972. Iron out-of-planarity and tetrapyrrole nitrogen nuclear spin state mixing in high-spin ferric haem. *Mol. Phys.* 24:787–800.
27. Scholes, C. P., A. Lapidot, R. Mascarenhas, T. Inubishi, R. A. Isaacson, and G. Feher. 1982. Electron nuclear double resonance (ENDOR) from heme and histidine nitrogens in single crystals of aquometmyoglobin. *J. Am. Chem. Soc.* 104:2724–2735.
28. Brill, A. S., and D. A. Hampton. 1979. Quantitative evaluation of contributions to electron paramagnetic resonance line widths in ferric hemoglobin single crystals. *Biophys. J.* 25:313–322.
29. Bialek, W., and R. F. Goldstein. 1985. Do vibrational spectroscopies uniquely describe protein dynamics? *Biophys. J.* 48:1027–1044.
30. Yim, M. B., L. C. Kuo, and M. W. Makinen. 1982. Determination of the zero-field splitting constants of high-spin metalloproteins by a continuous wave microwave saturation technique. *J. Mag. Res.* 46:247–256.